



HAL
open science

Orchestrating Communications in a Three-Type Chirality Totem: Remote Control of the Chiroptical Response of a Mobius Aromatic System

Rajaa Benchouaia, Nicolas Cisse, Bernard Boitrel, Matthieu Sollogoub, Stéphane Le Gac, Mickaël Ménand

► **To cite this version:**

Rajaa Benchouaia, Nicolas Cisse, Bernard Boitrel, Matthieu Sollogoub, Stéphane Le Gac, et al.. Orchestrating Communications in a Three-Type Chirality Totem: Remote Control of the Chiroptical Response of a Mobius Aromatic System. *Journal of the American Chemical Society*, 2019, 141 (29), pp.11583-11593. 10.1021/jacs.9b04074 . hal-02278394

HAL Id: hal-02278394

<https://univ-rennes.hal.science/hal-02278394>

Submitted on 14 Oct 2019

HAL is a multi-disciplinary open access archive for the deposit and dissemination of scientific research documents, whether they are published or not. The documents may come from teaching and research institutions in France or abroad, or from public or private research centers.

L'archive ouverte pluridisciplinaire **HAL**, est destinée au dépôt et à la diffusion de documents scientifiques de niveau recherche, publiés ou non, émanant des établissements d'enseignement et de recherche français ou étrangers, des laboratoires publics ou privés.

Orchestrating Communications in a Three-Type Chirality Totem: Remote Control of the Chiroptical Response of a Möbius Aromatic System

Rajaa Benchouaia,^{†,§} Nicolas Cissé,^{†,§} Bernard Boitrel,[†] Matthieu Sollogoub,[‡] Stéphane Le Gac*^{*,†} and Mickaël Ménand*^{*,‡}

[†] Univ Rennes, CNRS, ISCR (Institut des Sciences Chimiques de Rennes) – UMR 6226, Rennes F-35000, France

[‡] Sorbonne Université, CNRS, Institut Parisien de Chimie Moléculaire, IPCM (UMR 8232), F-75005 Paris, France

ABSTRACT: Among the various types of chirality (central, axial, helical, planar...), that inherent to Möbius topology remains almost unexplored, partly due to the difficulty to access Möbius compounds. Over the last decade, [28]hexaphyrins have revealed among the best candidates to build on Möbius aromaticity. Whereas their flexibility needs to be controlled to get P/M twist enantioselectivity, it could be of great interest to sustain dynamic chirality transfer. In this context, we report herein the first example of a Möbius aromatic ring capped by a cavity, consisting in a Möbius [28]hexaphyrin doubly-linked to an α -cyclodextrin. This unique design affords a “totem” of three different chirality elements arising from the cyclodextrin (fix central chirality), the bridging pattern (dynamic planar chirality) and the hexaphyrin (dynamic topological chirality). Chirality transfers (see TOC graphic) are characterized by a stereospecific planar-to-topological communication (diast. excess > 95 %; the highest asymmetric selectivity reported to date for a Möbius ring) combined to a stereoselective central-to-planar communication (up to 60 % diast. excess). Interestingly, the stereoselectivity is remotely controlled by coordination of an achiral effector to the hexaphyrin, increasing up to five times the chiroptical response of the Möbius aromatic π -system. These results highlight the advantageous use of dynamic chirality transfers to further incorporate Möbius chirality and aromaticity into all kind of stimuli responsive devices.

INTRODUCTION

The conversion of the artistically elegant Möbius strip topology into a molecular architecture has remained elusive until the pioneering report of Walba's bis-crown ether ribbon.^{1,2} Two decades later, Herges devised an ingenious multi-step approach to synthesize the first π -conjugated Möbius molecule derived from a benzo-fused annulene scaffold.³ Soon after, the groups of Latos-Grażyński⁴ and Osuka⁵ reported concomitantly the synthesis of heteroannulenic compounds with native Möbius twisted topologies. The conformational flexibility of these expanded porphyrinoids⁶ allowed to experimentally evidence the $4n$ π -conjugated “Möbius aromaticity”, unknown in nature but earlier predicted by Heilbronner.⁷ The straight forward access to regular *meso*-aromatic expanded porphyrins allowed to further investigate the influence of the Möbius twist on their physico-chemical properties ($4n+2$ antiaromaticity,⁸ Baird rules,^{9...}). However, despite important findings in this field, it is worth to note that the inherent chirality of Möbius compounds has remained quasi-unexplored.^{10,11} Considering the paramount importance of chirality in biological processes, drug design, material sciences and many other fields, scrutinizing Möbius chirality has become a major challenge with promising opportunities.¹²

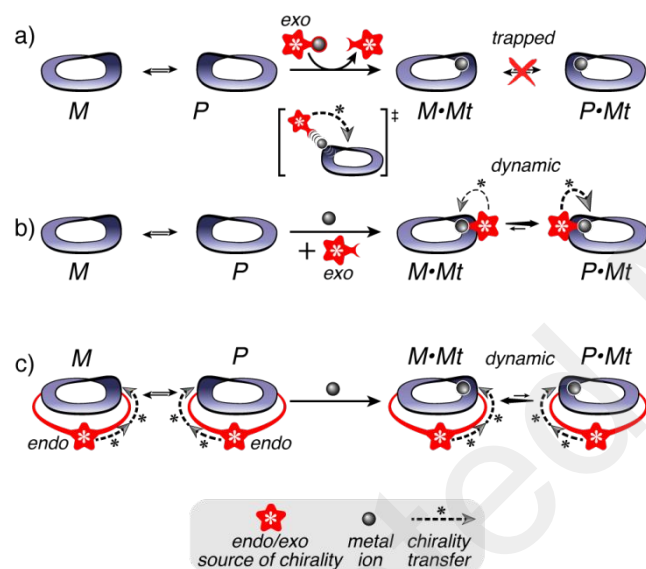
In general, Möbius conformations of regular expanded porphyrins are flexible, making their chiral π -conjugated system dynamic. Therefore, the fluxionality of the macrocycles needs either to be frozen or dynamically controlled to access optically active samples. Scheme 1 summarizes the few successful attempts of stereoselective formation of Möbius compounds, all involving a [28]hexaphyrin scaffold,¹³ and emphasizes the chirality transfers at work. Following the “frozen” strategy (Scheme 1a), kinetically trapped Möbius enantiomers were stereoselectively obtained using Pd(II) chiral salts, with however modest enantiomeric excess (23 % *e.e.*).^{10,14} On the other hand, the “stereodynamic” strategy allowed to control the Möbius twist winding to the highest diastereomeric excess reported to date (76% *d.e.*) using labile metal complexes associated with chiral ligands (Scheme 1b).¹¹ The dynamic stereocontrol¹⁵ of the Möbius twist can thus turn to be a major advantage for the development of responsive devices and materials with tuneable chiroptical and aromaticity properties. Moreover, switchable stereoisomerism is of particular interest in asymmetric catalysis or for the directional control of motion, which are key features for the design of smart molecular machines.¹⁶

To get any benefit from Möbius stereoisomerism, fine understanding of chirality transfer¹⁷ from or to other stereochemical elements is crucial. Inspired by recent findings

in chiral molecular switches and catalysts, featuring hybrid¹⁸ or compartmentalized¹⁹ transfer of chirality, we devised a new strategy where multiple stereochemical sources would be endogenous to a dynamic Möbius edifice (Scheme 1c). Having a flexible Möbius ring covalently connected to other chiral element(s) would offer a unique opportunity to study chirality transfer phenomena, and ultimately chiral induction of the Möbius twist.

We describe herein an unprecedented system composed of three different stereochemical elements arranged in a “totem” fashion referred as central (fix), planar (dynamic) and topological (Möbius, dynamic). Nuclear magnetic resonance (NMR) and electronic circular dichroism (ECD) spectroscopic investigations revealed effective chirality transfers across the three elements according to *stereoselective* and *stereospecific* relationships, with a possible remote control, leading ultimately to amplification of the chiroptical response of the Möbius aromatic π -system.

Scheme 1. Simplified depiction of different strategies achieving stereoselective Möbius winding.



(a) “Trapped” coordination approach with chirality transfer occurring in the transition state (23 % *e.e.*).¹⁰ (b) “Dynamic” coordination approach with an exogenous chiral ligand offering chirality transfer in the equilibrium of diastereomeric complexes (76 % *d.e.*).¹¹ (c) Present contribution: “fix” and “dynamic” endogenous chiral sources offering intramolecular chirality transfers in the final equilibrium of diastereomeric coordination complexes.

RESULTS AND DISCUSSION

Design

We recently described hexaphyrin-cyclodextrin hybrid compounds (HCDs) made of an hexaphyrin unit (the six-pyrrole homologue of porphyrin) attached to one or two A,C,E-modified α -cyclodextrin unit(s) by triple or sixfold covalent linkages (Figure 1b).²⁰ In these hybrids, the hexaphyrin unit adopts up to three different planar conformations (rectangle,

dumbbell, and triangle). For each of these, the two oxidation states of the hexaphyrin follow Hückel rules with aromatic character for the oxidized state “[26]” and antiaromatic character for the reduced one “[28]” ($4n+2$ and $4n$ conjugated π electrons, respectively). The three planar conformations are interconvertible in both oxidation states using various stimuli.²⁰ In the particular case of the triangular conformation, independently of the chirality of the cyclodextrin, the triple attachment on one face generates planar chirality (Figure 1b). Indeed, the 5,15,25 and 10,20,30 bridging patterns are mirror images and correspond to opposite R_p and S_p configurations.^{20b} Their equal population indicates a lack of stereodiscrimination from the cyclodextrin (static source of central chirality with 30 stereogenic centres, Figure 1a, bottom).²¹ The planar chirality is dynamic since the diastereomers are in equilibrium through coupled *in-out/out-in* inversions of the pyrroles (Figure 1a middle, for a related process).

Despite the plasticity of these hybrids, the Möbius aromatic conformation ([28] state) was not detected suggesting that a high strain penalty due to the triple covalent attachment prevents a twisted conformation. We thus turned our attention to less constrained doubly-linked HCDs using an A,D-difunctionalized cyclodextrin (Figure 1c). The devised ‘A,D’ pattern was expected to (i) generate planar chirality, (ii) favor Möbius conformation in the [28] state, and ultimately (iii) afford a 3-type chirality totem suitable for chiral transfers. Stereochemical analysis revealed up to 3 possible diastereomers for the most common rectangular conformation and 12 others for the Möbius hexaphyrin one (Figure 1c):

(i) the rectangular diastereomers differ by their three possible *meso*-bridging patterns, two of which generating planar chirality (Figure 1a, middle). Whereas the 5,20-*meso* bridged hexaphyrin affords an achiral short-side bridging pattern, bridging the 10,25 and 15,30-*meso* positions affords chiral long-side bridging patterns of opposite R_p/S_p configurations. The expected dynamic character of these *meso*-bridging patterns through coupled *in-out/out-in* inversions of the pyrroles,²⁰ would offer a possible dynamic control of the planar chirality owing to the cyclodextrin chirality.

(ii) introducing half-a-twist in the π -conjugated circuit gives rise to Möbius bands with opposite P/M handedness (Figure 1a top). Considering a simplified rectangular hexaphyrin, the twisting of an inverted pyrrole can process upward (blue arrows) or downward (red arrows) with either left or right orientations, leading to four twisted stereoisomers: two degenerate (C_2 -symmetrically related) M twists and P twists.²² Bridging opposite *meso* positions of these stereoisomers lifts their degeneracy affording two different M twists and two different P twists. These four Möbius conformations can occur for each of the three possible *meso* bridging patterns affording up to 12 possible diastereomers for the targeted ‘A,D’ doubly-linked HCDs (Figure 1c). Similarly to the rectangular conformation, planar chirality arises for the long-side bridging patterns (10,25 and 15,30), affording totems of three types of chirality (Figure 1c).

Importantly, the *meso*-substitution pattern and Möbius isomerization processes are governed by very different energy barriers. The Möbius twisting one amounts approximately for 8 kcal.mol⁻¹²³ while that of the dynamic planar chirality reaches 23 kcal.mol⁻¹.²⁴

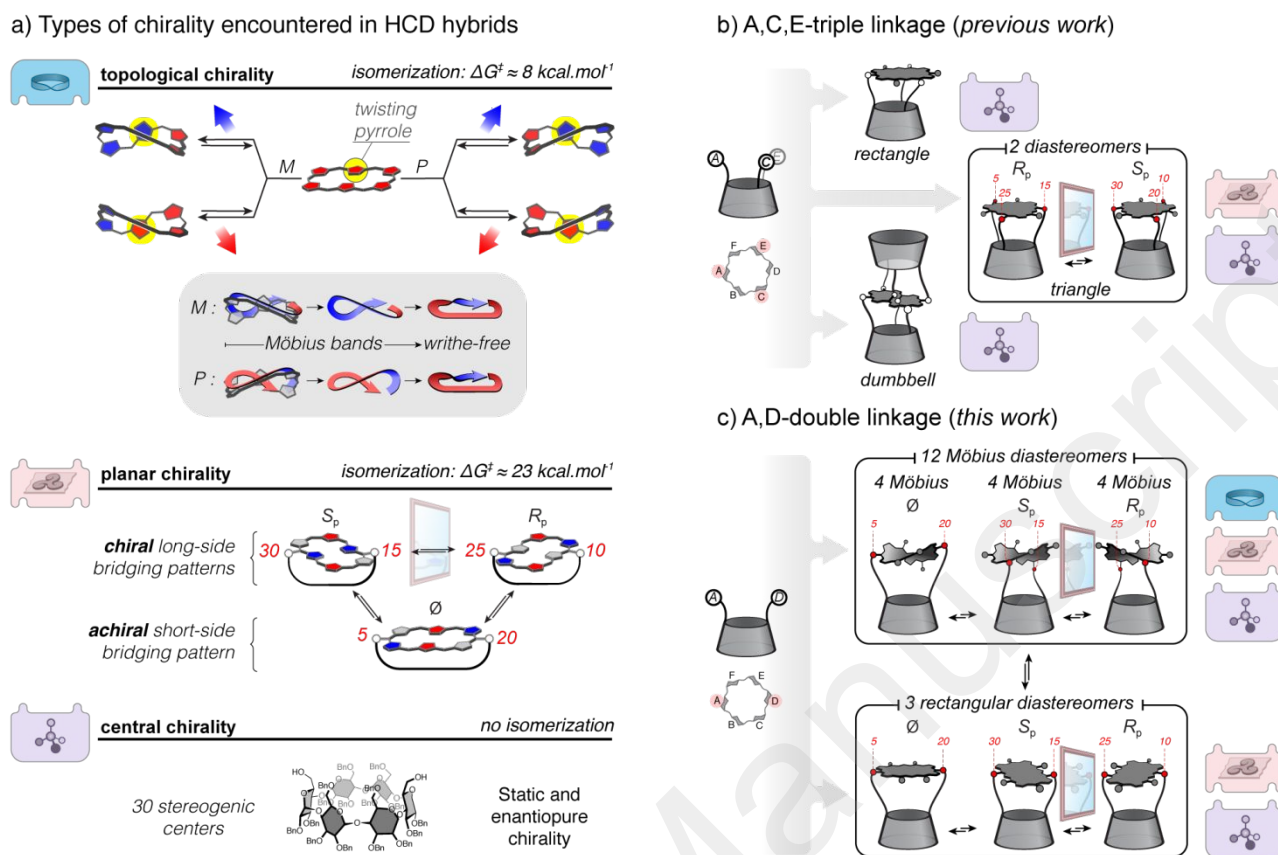


Figure 1. (a) Details of chiral elements constituting the targeted totem edifices: (bottom) representation of the α -cyclodextrin A,D-diol embedding 30 stereogenic centers which are thermodynamically and kinetically stable; (middle) illustration of the dynamic planar chirality arising from bridging the 10,25 and 15,30 *meso*-positions of a rectangular hexapyrin. The bridging pattern isomerization occurs through coupled *in-out/out-in* pyrrole inversions. The labelling of the *meso*-substitution patterns is defined clockwise relative to a short side substituent (labelled 5) considering the free face of the hexapyrin; (top) illustration of the equilibria between four possible Möbius stereoisomers (transiting through a rectangular conformation), depending on the *up/down* and *right/left* twisting of an inverted pyrrole (highlighted in yellow and converted to blue and red plain arrows). Note that the same degenerate isomerization process is obtained using the opposite inverted pyrrole at the front. The chirality of the Möbius strip is emphasized both with the native writhe view and the stretched writhe-free view of the Möbius strip (grey box). (b) Overview of the triply-linked hexapyrin-cyclodextrin (HCD) hybrids and their accessible hexapyrin conformations.²⁰ Inset: stereochemical analysis of the two diastereomers of the triangular HCD exhibiting planar and central chirality. (c) Stereochemical analysis of the targeted totem design of a three-stereogenic elements assembly from doubly-linked HCD hybrids.

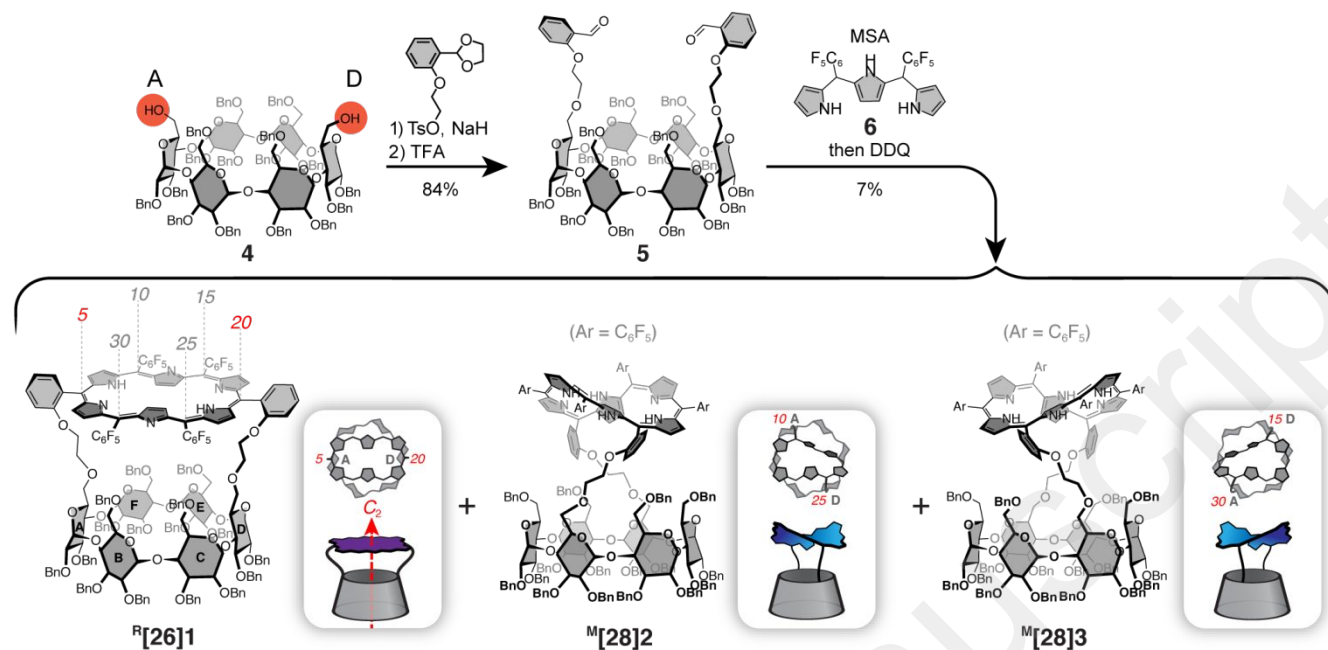
Synthesis and characterization

The synthesis of the doubly-linked HCD hybrids was performed using precursor **5** obtained by alkylation-deprotection of the perbenzylated α -cyclodextrin 6A,6D-diol **4**²⁵ in 84% yield over two steps (Scheme 2). This dialdehyde was further engaged in an acid catalyzed macrocyclization with two equivalents of tripyrrane **6**,^{6h} followed by an *in-situ* oxidation with 2,3-dichloro-5,6-dicyano-1,4-benzoquinone (DDQ). Subsequent purification of the crude material by column chromatography afforded a turquoise blue fraction (^M[**28**]**2** and ^M[**28**]**3**) and a more polar violet fraction (^R[**26**]**1**) (Scheme 2). High resolution mass spectrometry (HRMS) analyses were indeed consistent with the formation of doubly-linked HCD hybrids with 28 and 26 π electron systems, respectively. The UV-vis-NIR absorption spectra of both blue and violet fractions showed similar

absorption profiles, with an intense Soret-like band at respectively 601 and 577 nm and four Q-like bands spanning up to the NIR region, characteristic of an aromatic character (Figure 2). These features are consistent with a Hückel aromatic character for ^R[**26**]**1** ($4n+2$ π electrons, planar) and a Möbius aromatic one for ^M[**28**]**2**/^M[**28**]**3** ($4n$ π electrons, singly twisted). The ¹H NMR spectrum of ^R[**26**]**1** recorded in CDCl₃ displays a well-resolved pattern corresponding to a C_2 -symmetric compound (SI). The chemical shifts of the β -pyrrolic protons ($\beta\pi$) are splitted into two characteristic regions evidencing a strong diatropic ring current. The shielded part displays a broad singlet (-1.58 ppm, NH_{in}) and two doublets (-2.70 and -2.95 ppm, $\beta\pi_{in}$), while the deshielded one shows four doublets (9.23, 9.20, 9.12 and 9.02 ppm, $\beta\pi_{out}$). Such a distribution is consistent with a C_2 -symmetric rectangular conformation orienting two NH and four $\beta\pi$ protons in the shielding inner part

of the macrocycle while the deshielding periphery comprises eight $\beta\pi$ protons. The linkers connecting the cyclodextrin to the

hexaphyrin were found to be located on both



Scheme 2. Synthesis of HCD hybrids $R[26]1$, $M[28]2$ and $M[28]3$. Labeling for all isomers follows the nomenclature provided on compound $R[26]1$.

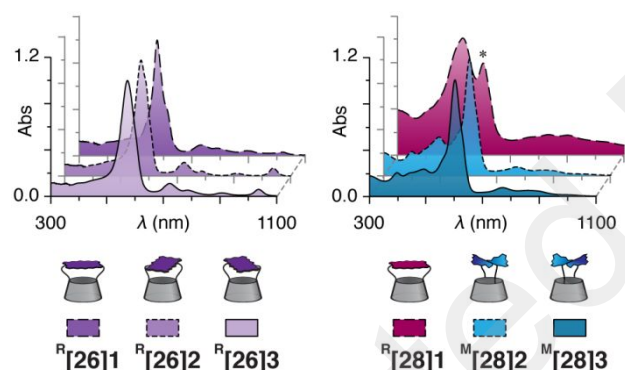


Figure 2. Normalized UV-vis-NIR absorption spectra in CH_2Cl_2 of $R[26]1$, $R[26]2$, $R[26]3$, $R[28]1$, $M[28]2$ and $M[28]3$. (*) contamination with $M[28]2$ and $M[28]3$.

short sides of the hexaphyrin rectangle (5,20 *meso*-positions, Scheme 2) as deduced from an unusual ^{19}F - ^{19}F through space coupling.²⁶ Indeed, this substitution pattern brings the *meso*-pentafluorophenyl groups on the long sides of the rectangle. Hence, two *ortho*-fluorine atoms (one of each adjacent *meso*-pentafluorophenyl groups) are in close proximity leading to the coupling/correlation observed in both ^{19}F and 2D ^{19}F - ^{19}F COSY NMR spectra (SI). In addition, two O6-benzyl groups belonging to the C_2 -symmetrically related C and F glucose units undergo a marked shielding effect consistent with their location into the confined space between the hexaphyrin and the primary rim of the cyclodextrin. In contrast, the ^1H NMR spectrum (CDCl_3 , 300 K) of the turquoise blue fraction reveals two C_2 -symmetric compounds ($M[28]2$ and $M[28]3$) in a roughly 1:1 ratio, not separated by silica gel chromatography (SI). Whereas sharp signals are observed for the cyclodextrin parts, most of the

hexaphyrin protons are strongly broadened over a large temperature range (183 K to 330 K) preventing direct determination of its conformation. Such a behaviour is consistent with an equilibrium occurring on the NMR time scale between Möbius conformations, notably between C_2 -symmetrically related ones (degenerate conformations).^{5,27} Indeed, the energy barrier associated to Möbius conformational exchange is about 8 kcal.mol⁻¹ (Figure 1a, top).²³ As determined below, $M[28]2$ and $M[28]3$ differ by their bridging patterns which are respectively 10,25 and 15,30 (Scheme 2), affording planar chirality (Figure 1c).

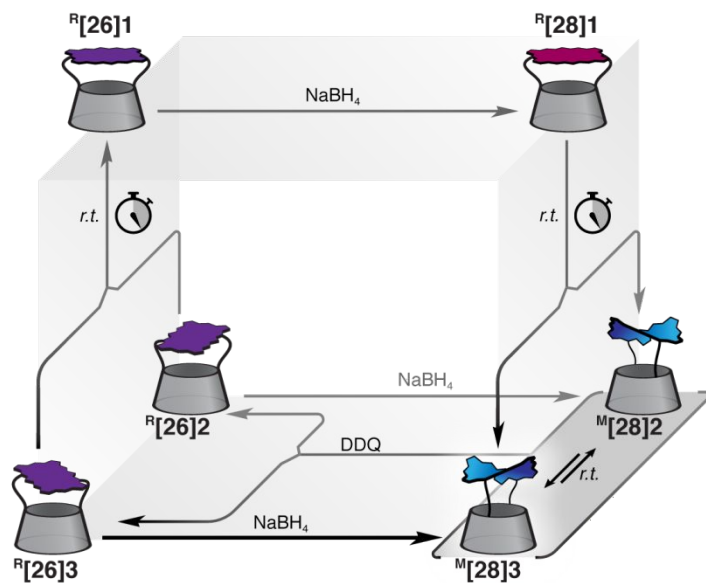
Redox conversion and conformational isomerization

To further study $M[28]2$ and $M[28]3$, we decided to explore their oxidized counterparts. Thus, DDQ oxidation of the mixture of $M[28]2$ and $M[28]3$ allowed to isolate pure $R[26]2$ and $R[26]3$ by chromatography (Scheme 3). Both UV-vis-NIR absorption spectra display absorption bands in accordance with an aromatic character (Figure 2). The ^1H NMR signatures of both C_2 -symmetric compounds were very similar to that of $R[26]1$ with three shielded signals ($2\times\text{NHin}$ and $4\times\beta\text{pin}$), four deshielded ones ($8\times\beta\text{out}$), and showing two included benzyl groups belonging to the cyclodextrin primary rim (SI). Therefore, the hexaphyrin unit of $R[26]2$ and $R[26]3$ also adopts a rectangular conformation. Yet, these hybrids differ from $R[26]1$ by their bridging pattern, respectively 10,25 and 15,30 (Scheme 3b, *vide infra*).²⁸ Besides, $R[26]2$ and $R[26]3$ are unstable in solution at room temperature, isomerizing into the thermodynamically more stable $R[26]1$ isomer (Scheme 3a and Figure 1a middle, SI). Energy barriers of 25.8 and *ca.* 25.4 kcal.mol⁻¹ were estimated for the conversion of $R[26]2$ and $R[26]3$ into $R[26]1$, respectively (SI).

Conversely, reduction of $R[26]1$ with NaBH_4 in $\text{THF-}d_8$ did not produce the former mixture of $M[28]2$ and $M[28]3$ but rather a

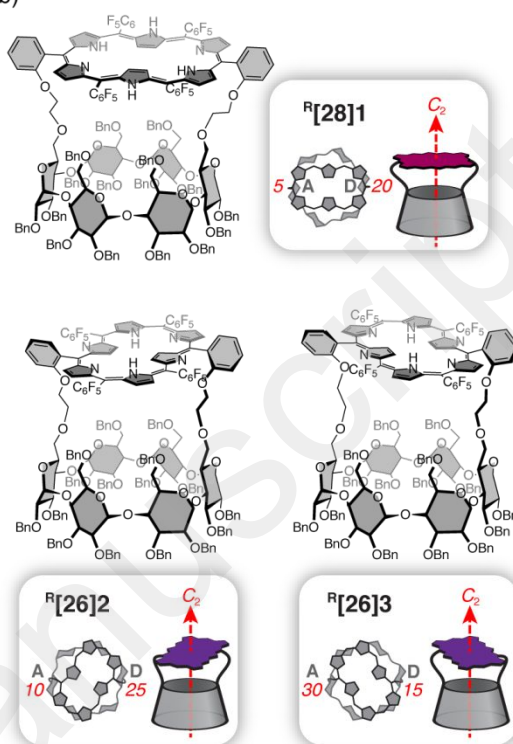
red-brown product ($R^1[28]1$, Scheme 3) exhibiting a broad absorption spectrum in line with an antiaromatic character (Figure 2).²⁹ Its C_2 -symmetric 1H NMR pattern (SI) confirms a

a)



rectangular conformation, with a characteristic reversed splitting of

b)



Scheme 3. (a) Global synthetic network connecting $R^1[26]1$, $R^1[26]2$, $R^1[26]3$, $R^1[28]1$, $M^1[28]2$ and $M^1[28]3$. (b) Structures of $R^1[28]1$, $R^1[26]2$ and $R^1[26]3$.

the $\beta\pi$ proton resonances compared to the aromatic $R^1[26]1$ isomer. Indeed, the paratropic ring current induces a downfield shift of the four inner $\beta\pi$ protons (14.91 and 14.67 ppm), and an upfield shift for the eight outer ones (3.89, 3.91, 4.71 and 4.82 ppm). $R^1[28]1$ isomer is also unstable in solution (THF- d_8) at room temperature, isomerizing into the Möbius aromatic mixture of $M^1[28]2$ and $M^1[28]3$ (Scheme 3a, SI). This process is consistent with a short-side 5,20 *meso*-bridging pattern in $R^1[28]1$ (retained upon reduction of $R^1[26]1$), that converts almost equally into the 10,25 and 15,30 long-side ones, coupled to a rectangular-to-Möbius isomerization (Figure 1a, middle and top). It has to be noted that the more rigid triply-linked [28]HCD derivative affords a stable rectangular antiaromatic conformation.^{20a,30} In contrast, the doubly-linked [28]HCD recovers enough flexibility to incorporate a twist into the π -conjugated macrocycle.

Knowing the redox interconversion and equilibration pathways, we were able to devise a synthetic strategy to access $M^1[28]2$ and $M^1[28]3$ separately. Therefore, we first oxidized an equilibrated mixture of $M^1[28]2$ and $M^1[28]3$ with DDQ and the corresponding $R^1[26]2$ and $R^1[26]3$ were separated by column chromatography. Their reduction with $NaBH_4$ gave isolated samples of $M^1[28]2$ and $M^1[28]3$ with respectively 90:10 and 15:85 diastereomeric ratio (*d.r.*). Their equilibration proceeds slowly at room temperature, thermodynamic ratio (55:45) being reached upon heating overnight at 60 °C (SI). To the best of our knowledge, $M^1[28]2$ and $M^1[28]3$ are the first examples of cavity-capped Möbius molecular rings.

Chirality induction and chiroptical properties with free bases

We next examined the chiroptical properties of $M^1[28]2$ and $M^1[28]3$ by ECD spectroscopy.³¹ Interestingly, these isolated compounds exhibit mirror ECD spectra with intense bis-signate Cotton effect in the Soret band wavelength region (Figure 3). These signatures are

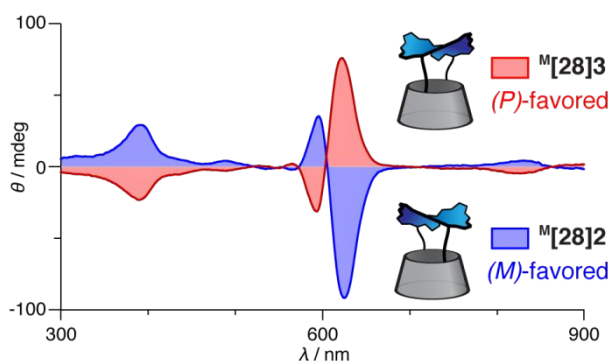


Figure 3. Electronic circular dichroism spectra in $CHCl_3$ of diastereomerically enriched $M^1[28]2$ (blue) and $M^1[28]3$ (red) (respectively 90:10 and 15:85 *d.r.*; intensities scaled according to

their corresponding UV-vis absorption spectra normalized at their maximum absorbance).

in good agreement with those of optically pure Möbius hexaphyrin metal complexes,¹⁰ and give us four main informations:

(i) the intense chiroptical response suggests that a high *P/M* stereoselectivity occurs at the level of the Möbius twist, although quantitative assessment cannot be achieved at this stage due to the dynamic character of the Möbius conformation;

(ii) the stereoselectivity of the Möbius twist originates from the 10,25/15,30 bridging patterns (opposite *R_p/S_p* planar configurations), without noticeable influence of the chirality of the cyclodextrin. Indeed, the ECD spectrum of the equilibrated ^M[28]2 and ^M[28]3 mixture (*ca.* 1:1 thermodynamic ratio) exhibits a weak signal;

(iii) compared to native [28]hexaphyrins, the bridging to the cyclodextrin leads to a significant increase of the *M* twist ↔ *P* twist isomerisation barrier. Actually, Möbius isomerization is mainly if not entirely coupled to the planar isomerization process (Figure 1a, top and middle). This gives a unique opportunity to isolate optically active Möbius hexaphyrins in their free base forms;

(iv) the negative (/positive) Cotton effect for ^M[28]2 (^M[28]3) allows to assign the absolute configurations of the Möbius twists by comparison with isolated enantiopure Möbius hexaphyrins, giving *M* for ^M[28]2 and *P* for ^M[28]3.^{10,32} This further enable to assign the 10,25 (*R_p*) and 15,30 (*S_p*) bridging patterns to ^M[28]2 and ^M[28]3 and to their oxidized forms ^R[26]2 and ^R[26]3.

Indeed, each bridging pattern can formally generate four diastereomeric Möbius conformations, two *M* twists and two *P* twists (Figure 1a top and 1c). Molecular modelling of the different possible isomers evidenced that only a single one fits a given planar configuration (SI). Figure 4 illustrates the case of the *M* twist for both 10,25 and 15,30 bridging patterns (^M[28]2 and ^M[28]3 respectively). While ^M[28]2 isomers adopt a global expanded and strain-relieved geometry, the ^M[28]3 ones are more compact and constrained (Figure 4, A and B vs. C and D). These contrasting geometries are imposed by the relative orientation of the *meso*-substituents adjacent to the *twisted* pyrrole (in red/yellow). Actually, the twisting process projects these *meso*-substituents (*meso*-C₆F₅ and *meso*-aromatic linker) in opposite directions (*up* and *down* compared to the hexaphyrin mean plane). In the case of ^M[28]2, the *meso*-C₆F₅ (in blue, Figure 4a) is oriented upward and away from the cyclodextrin while the *meso*-aromatic linker is oriented downward pointing the ethylenic spacer towards the cyclodextrin. This situation leads to the observed strain-relieved geometries and is thus favored. In contrast, ^M[28]3 orients the *meso*-C₆F₅ downward leading to steric interactions with the cyclodextrin (Figure 4b). These interactions are amplified by the highly compressed geometries arising from the upward orientation of the *meso*-aromatic linker which forces the hexaphyrin part to come closer to the cyclodextrin one, thus leading to unfavored geometries. Conversely, the *P* twist fits better the 15,30 bridging pattern of the ^M[28]3 isomer than the 10,25 one of ^M[28]2 (SI).

This stereochemical study evidences a strong communication between the planar and Möbius stereogenic elements, but also shows a weak one (if any) with the cyclodextrin's chirality (no

stereoselectivity between ^M[28]2 and ^M[28]3 of opposite planar configuration). Targeting a full communication across the three levels of this chiral totem, we next investigated the effect of conformational restriction of the Möbius hexaphyrin upon coordination.

Metalation with Zn(II): a three-type chirality totem in action

Dynamic character of the metal complexes

Coordination studies with ^M[28]2 and ^M[28]3 focused on the complexation of a labile metal ion, *i.e.* Zn(II), in order to

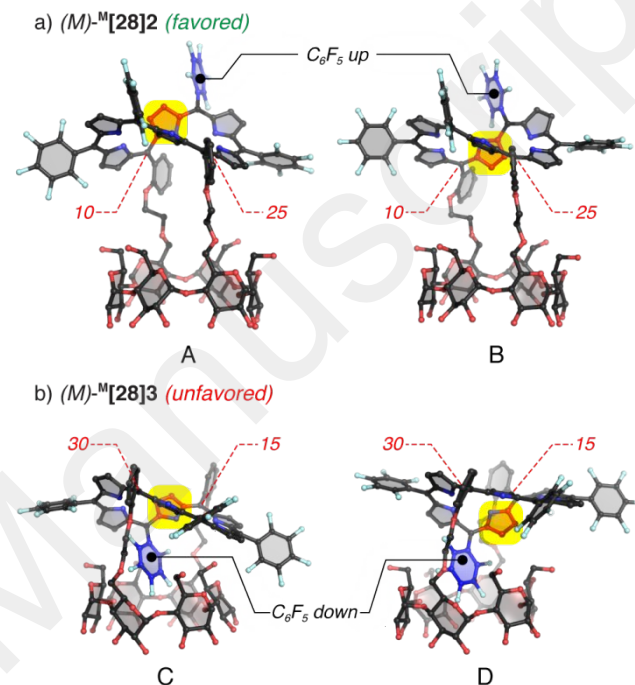
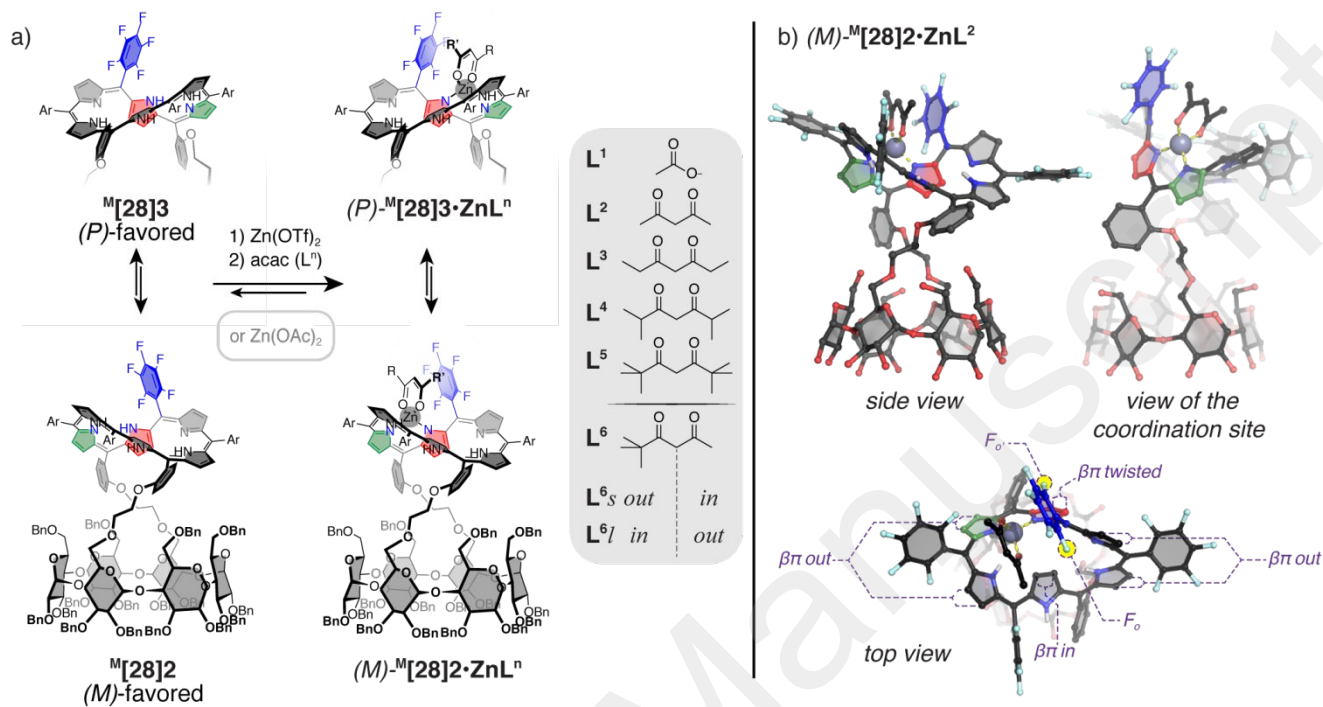


Figure 4. Optimized geometries of the two *M* Möbius isomers for (a) ^M[28]2 and (b) ^M[28]3 (Avogadro software, UFF parameters; benzyl groups were omitted for modelling). *Twisted* pyrroles are highlighted in red/yellow and *meso*-C₆F₅ substituents adjacent to the *twisted* pyrroles are highlighted in blue.

provide conformational restriction to the Möbius ring while keeping the isomerization processes possible (see also approaches “b” and “c” in Scheme 1). Acetate (L¹) and a set of acetylacetonate (acac derivatives: L²-L⁶) ligands were used to probe steric factors around the metal (Scheme 4a). Coordination properties were first assessed by ¹H NMR titration experiments with either Zn(OAc)₂ or Zn(OTf)₂/L² in CDCl₃/CD₃OD (9:1) mixture. ^M[28]2 and ^M[28]3 were used in various *d.r.* ratios (90:10, 55:45 and 15:85) to evaluate the dynamics of the metal complexes (SI).³³ All cases led to the same final mixture of mononuclear Möbius complexes with a 4:1 thermodynamic ratio of (*M*)-^M[28]2•ZnL¹⁻² and (*P*)-^M[28]3•ZnL¹⁻² respectively (Scheme 4a). Interestingly, the intermediate mixtures of Zn(II) complexes equilibrate rapidly (*ca.* one hour at 298 K), the most striking example being the rapid *S_p* → *R_p* planar isomerization occurring with the starting ^M[28]3 enriched sample. These observations highlight the dynamic character of both the topological and planar chiralities of the complexes.

Structure elucidation of the metal complexes

In contrast with the free bases, the *major* and *minor* Zn(II) complexes display well-defined 1D and 2D NMR spectra (SI) with characteristic patterns of “frozen” Möbius conformations on the NMR time scale. For instance, both L²-type complexes show three sets of resonances for the βπ protons due to the diatropic ring current. These sets correspond to three main



Scheme 4. (a) Zn(II) coordination with $M[28]2/M[28]3$ (Ar = C₆F₅) and the ligands (Lⁿ) used in this study. (b) Optimized geometry with different views of (M) - $M[28]2 \cdot ZnL^2$ (Avogadro software, UFF parameters; benzyl groups were omitted for modelling).

vs. 0.21 to 0.72 ppm for the three others, SI). In agreement with the literature, this shielding corresponds to a *meso*-C₆F₅ adjacent to the *twisted* pyrrole and projected towards the Möbius ring (Scheme 4, in blue), the three other *meso*-C₆F₅ being peripheral.³⁴ Moreover, two benzylic groups on the primary rim of the cyclodextrin unit experience a marked shielding ($\Delta\delta$ up to ~4 ppm), indicating that they occupy the confined space between the hexaphyrin and the cyclodextrin units. For each complex, we determined the preferred Möbius stereoisomer among the four possible ones (Figure 1a) following converging evidences:

(i) oxidation of the Zn(II) complexes led to a mixture enriched with $R[26]2$ (SI). Since DDQ oxidation carried out on the corresponding free bases did not affect the 1:1 ratio of planar isomers, this observation indicates that $M[28]2 \cdot ZnL^n$ is the *major* species and $M[28]3 \cdot ZnL^n$ is the *minor* one;

(ii) ECD spectra analysis indicate that the favored *M* and *P* Möbius configurations of the free bases are retained upon Zn(II) complexation (see discussion below);

(iii) L¹-type complexes are characterized by a broad signal (-0.93/-1.08 ppm, *minor/major* species) corresponding to the methyl group of a bound acetato ligand (Figure 5a).³⁵ Their complexation induced shifts (CIS: $\Delta\delta_{Me} \sim -3$ ppm, Table 1) indicate that these ligands face the inner part of the Möbius hexaphyrin. In contrast, the two methyl groups of the *acac* ligand display very different CIS for both the *minor* and the

pyrrole orientations (Scheme 4b): *in* (2H: -2.54/-1.28 and -1.98/-1.10 ppm), *twisted* (2H: 4.94/4.94 and 4.48/4.73 ppm) and *out* (8H: 7.15 to 8.30 ppm). Besides, the ¹⁹F NMR patterns of both *major* and *minor* species evidence an important shielding of a single *ortho*-fluorine atom belonging to a *meso*-C₆F₅ ($\Delta\delta[ortho] = 4.49$ ppm

major L²-type complexes ($\Delta\delta_{Me} \sim -3$ and -0.8 ppm; Figure 5b, Table 1, SI). It suggests that L² binds the metal with an off-centred position from the Möbius ring, orienting a methyl group closer to the ring than the other (Scheme 4b). Importantly, both L¹- and L²-type complexes (and even crowded L³⁻⁶-types, *vide infra*) did not afford any NOE correlations between bound ligands and either the introverted benzyl groups, the bridging linkages, or the cyclodextrin protons. This is consistent with an *exo*-coordination of the ‘ZnLⁿ’ moiety orienting the Lⁿ ligand away from the cyclodextrin unit,³⁶ the confined space between the hexaphyrin and the cyclodextrin units being occupied by benzyl groups. These observations corroborate the *down* orientation of the *twisted* pyrrole pointing the coordinating N atom *up*, and rules out the opposite orientation (Figure 4 “B” vs. “A” for (M) - $M[28]2$). Indeed, we recently showed that a capped hexaphyrin in Möbius conformation coordinates ‘ZnOAc’ at a dipyrin site involving the adjacent *twisted* and *out* pyrroles.¹¹ In the present case, the NMR and ECD data are in accordance with a similar tetrahedral coordination geometry depicted in Scheme 4 (red and green pyrroles). The metalation process thus corresponds to the stereoselective formation of (M) - $M[28]2 \cdot ZnL^n$ and (P) - $M[28]3 \cdot ZnL^n$ out of 12 possible diastereomers (Figure 1c).

Three-level chirality amplification

The chiral induction of the Möbius twist was further evidenced by ECD analysis. The ECD spectra of the NMR tube solutions containing ~4 :1 mixtures of (*M*)- $M[28]2\cdot ZnL^{1-2}$ and (*P*)- $M[28]3\cdot ZnL^{1-2}$ display up to 5 times higher intensity compared to the starting free base mixture (Figure 6). This corresponds formally to a shift from *ca.* 10 % to 56 and 60 % *d.e.* according to NMR integrations. These results highlight a rare case of configurationally responsive Möbius aromatic π -system exhibiting an *in-situ* enhancement of its chiroptical activity.¹¹

The amplification of the $M[28]2/M[28]3$ ratio (1:1 to 4:1) is a consequence of a coordination-driven communication between the static source of chirality (cyclodextrin) and the dynamic ones (the bridging linkages and the hexaphyrin). At first glance, the metal acts as an achiral effector which simply freezes the Möbius ring and strengthens the communication in the totem (Figure 7). As a result, two different stereoselection processes occur: (i) at the lower-half, the central chirality of the cyclodextrin partially discriminates the planar stereoisomers (*d.e.* ~ 60 %) and (ii) at the upper-half, the planar chirality drastically discriminates the Möbius stereoisomers affording a single twist for each bridging pattern of the Zn(II) complexes. Integrations of the well resolved ¹H NMR spectra indicate that this upper-half stereoselectivity for a Möbius twist is above 95 % *d.e.* for both *major* and *minor* complexes [(*M*) for $M[28]2\cdot ZnL$ and (*P*) for $M[28]3\cdot ZnL$].³⁷ This is the highest chiral induction value reported to date for a Möbius molecular ring (Scheme 1a,b).^{10,11} Importantly, it highlights a *stereospecific* relationship between the planar and Möbius chiralities, that undergo concomitant amplification processes ($P \rightarrow M$ Möbius twist induction coupled to $Sp \rightarrow Rp$ planar induction) (Figure 7, blue and red arrows).

Tuning chirality amplification using achiral effectors

Zn(II)-driven chiroptical responsiveness was further studied with different acac derivatives (Scheme 4a). Symmetrical ones (L^3 - L^5) behave similarly to L^1 and L^2 ligands affording a *major* [(*M*)- $M[28]2\cdot ZnL^{3-5}$] and a *minor* species [(*P*)- $M[28]3\cdot ZnL^{3-5}$] (Figure 5c-e, SI).³⁸ In line with L^2 , half of the bound L^3 - L^5 ligands is strongly shielded ($\Delta\delta$ up to 3.06 ppm, Table 1) in agreement with an off-centred binding geometry (Scheme 4a). Interestingly, the ratio of (*M*)- $M[28]2\cdot ZnL^{2-5}$ and (*P*)- $M[28]3\cdot ZnL^{2-5}$ strongly depends on the ligand size (Figure 5b-e, Table 1), the highest ratio being obtained for L^2 (R = Me, 78:22) and the lowest one for L^5 (R = *t*Bu, 60:40). This difference in chiral induction is nicely confirmed by ECD analysis of the NMR tube solutions showing the highest chiroptical activity for L^2 and a decreasing chiral induction with bulkier substituents (Figure 6).

The linear relation between the *d.e.* values measured from ¹H NMR integrations and the ECD intensity (Figure 6, right) indicates a chiroptical response influenced only by the *P/M* ratio. Thus, increasing steric congestion around the bidentate ligand leads to counter-intuitive effects: it weakens chirality transfer with the cyclodextrin (central-to-planar, lower-half communication), but does not affect the stereospecific relationship between planar and Möbius elements (upper-half communication). This ligand is thus acting as an achiral effector affording remote control^{39,40} across the whole totem and matching the piled chiral elements (Figure 7, green/purple arrows).

Table 1. Diastereomeric ratios for (*M*)- $M[28]2\cdot ZnL^n/(P)$ - $M[28]3\cdot ZnL^n$ and the corresponding CIS ($\Delta\delta$) of L^n .

L^n	R/R' ^a	<i>d.r.</i> ^b	$\Delta\delta$ (ppm) ^c				
			<i>M/P</i>	β^{in}	α^{in}	α^{out}	β^{out}
L^1		80:20	<i>M</i>	n.a. ^e	-3.06	n.a.	n.a.
			<i>P</i>	n.a.	-2.91	n.a.	n.a.
L^2	Me/Me	78:22	<i>M</i>	n.a.	-3.15	-0.84	n.a.
			<i>P</i>	n.a.	-3.01	-0.79	n.a.
L^3	Et/Et	72:28	<i>M</i>	-2.80	-3.06 ^d	-0.89 ^d	-0.47
			<i>P</i>	-2.77	-2.89 ^d	-0.83 ^d	-0.42
L^4	<i>i</i> Pr/ <i>i</i> Pr	67:33	<i>M</i>	-2.55 ^d	-2.80	-0.88	-0.50 ^d
			<i>P</i>	-2.74 ^d	-2.64	-0.85	-0.47 ^d
L^5	<i>t</i> Bu/ <i>t</i> Bu	60:40	<i>M</i>	-2.30	n.a.	n.a.	-0.45
			<i>P</i>	-2.26	n.a.	n.a.	-0.43
L^{6s}	Me ⁱⁿ / <i>t</i> Bu ^{out} (5%)	82:18	<i>M</i>	n.a.	-2.84	n.a.	-0.50
			<i>P</i>	n.a.	-2.74	n.a.	-0.47
L^{6l}	<i>t</i> Bu ⁱⁿ /Me ^{out} (95%)	62:38	<i>M</i>	-2.49	n.a.	-0.74	n.a.
			<i>P</i>	-2.42	n.a.	-0.70	n.a.

^a R and R' refers to the acac ligands with *in* and *out* indicating their relative orientations in the case of dissymmetrical acac. Proportions between brackets indicate the relative proportion of L^{6s} vs. L^{6l} .

^b *M/P d.r.* refers to (*M*)- $M[28]2\cdot ZnL^n/(P)$ - $M[28]3\cdot ZnL^n$ ratio deduced from ¹H NMR integration (experimental error: \pm 3%).

^c $\Delta\delta = \delta_{free} - \delta_{bound}$; α and β refer to the position relative to the carbonyl function.

^d Average value of diastereotopic protons.

^e n.a.: not applicable.

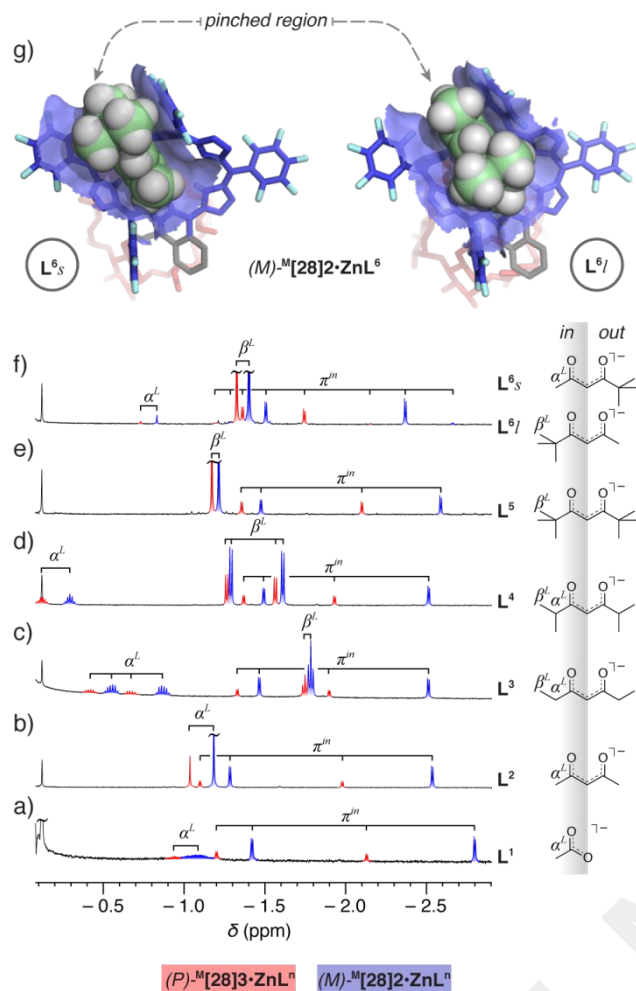


Figure 5. ¹H NMR spectra (CDCl₃/CD₃OD 9:1, 298 K, 500 MHz, high field region) of complexes (M)-M[28]2•ZnLⁿ/(P)-M[28]3•ZnLⁿ: (a) to (f), respectively L¹ to L⁶. α^L and β^L stand for the shielded protons of the ligand substituents. πⁱⁿ stands for the β-pyrrolic protons of the pyrrole *in*. (g) Optimized geometries of L^{6l} and L^{6s} isomers of (M)-M[28]2•ZnL⁶ (Avogadro software, UFF parameters, benzyl groups were omitted for modeling; top views with partial mapping of the Connolly solvent-accessible surface areas, L^{6l} and L^{6s} in space filling).

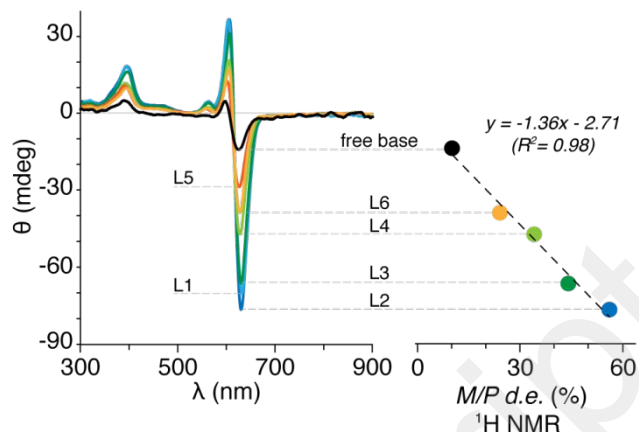


Figure 6. (left) ECD spectra in 9:1 CHCl₃/CH₃OH of equilibrated mixture of M[28]2/M[28]3 (free base) and of complexes (M)-M[28]2•ZnLⁿ/(P)-M[28]3•ZnLⁿ (L¹-L⁶) (ECD spectra obtained from NMR tube solutions and scaled according to their corresponding UV-vis absorption spectra normalized at their maximum absorbance). (right) Plot of the maximum ECD intensity vs. the M/P diastereomeric excess obtained from ¹H NMR integrations, showing a linear relationship (L², L³, L⁴, L⁶ plotted since quasi-quantitative metalation was achieved, *i.e.* > 90 %; L¹ and L⁵ not plotted since metalation was not complete; L⁶ corresponds to L^{6l} only).

To get further insights in the ligand crowding, we selected a dissymmetrical *acac* derivative L⁶ (R = Me, R' = *t*Bu) to evaluate the influence of the bulkiness orientation, *towards* or *outwards* the Möbius ring. Four complexes were obtained, corresponding to the (M)-M[28]2•ZnL^{6l}/(P)-M[28]3•ZnL^{6s} mixture of each of the two possible orientations of the dissymmetrical ligand (Scheme 4a and Figure 5f). Surprisingly, the major complexes (strong pair, 95 %) correspond to those orienting the largest substituent towards the ring (*tBu*_{in}: L^{6l}) while the minor ones (weak pair, 5 %) correspond to the smallest (*Me*_{in}: L^{6s}). Molecular models of L^{6l} and L^{6s} complexes (Figure 5g) suggest a pinched region due to the “*twisted*” *meso*-C₆F₅ (in blue in Scheme 4), leading to steric hindrance with the *tBu*_{out} of L^{6s}. Interestingly, the stereoselectivity ratios contrast with the stability ones. Indeed, the (M)-M[28]2•ZnL^{6l}/(P)-M[28]3•ZnL^{6s} ratios are 82:18 in the L^{6s} weak pair and 62:38 in the L^{6l} strong pair. These ratios fit those obtained with the corresponding symmetrical ligands L² and L⁵, respectively. Combined together, the stability of the complex is governed by the size of the *outward* substituent (the smallest the size, the highest the stability), while the stereoselectivity is governed by the size of the *inward* one (the smallest the size, the highest the stereoselectivity). This study shows that subtle steric effects occurring on the naked side of the Möbius ring have important consequences on the bridging pattern that is further discriminated by the cyclodextrin. In other words, coordination-induced freezing of the Möbius ring is a prerequisite, but is not enough to establish an efficient communication between the cyclodextrin and the planar chiralities. The exogeneous ligand plays a main role as well through an unexpected steric complementarity with the Möbius ring.

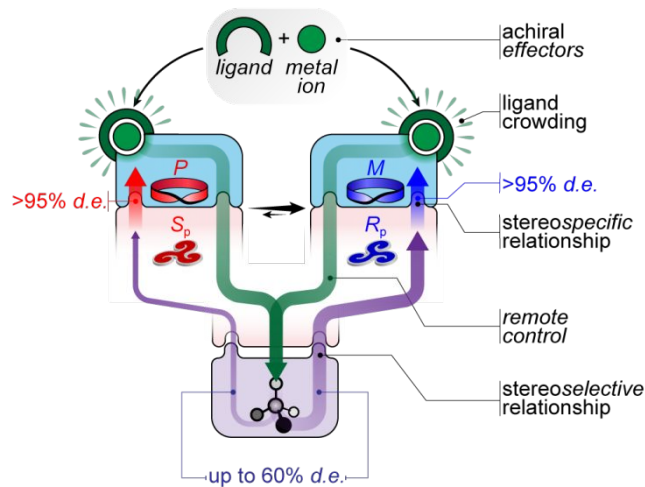


Figure 7. Cartoon of the chiral amplification chain in the totem HCD edifices.

CONCLUSION

A series of six new hexaphyrin-cyclodextrin hybrids has been developed and fully characterized, leading to three main results:

i) compared to the previous triply-linked hybrids, the double linkage favors the Möbius conformation in the 28π state, $^M[28]2$ and $^M[28]3$ being the first examples of a Möbius ring capped by a cavity. Free base hexaphyrins of opposite P/M twist could be isolated thanks to a fine understanding of the complex conformational and redox network connecting each of the six hybrids.

ii) chiral information is conveyed across these three-type chirality totems thanks to a subtle relay involving two dynamic chirality transfers (Figure 7). Spectacularly, the chiral relay occurring between the bridging pattern and the Möbius hexaphyrin is highly efficient affording a single out of four Möbius twists for a given bridging pattern. This illustrates an unprecedented planar-to-topological stereospecific relationship. On the other hand, the chiral relay between the cyclodextrin and the bridging pattern occurs only upon Zn(II) metalation of the Möbius hexaphyrin. The corresponding central-to-planar stereoselectivity is then tuned by an

exogenous ligand bound to the metal ion, acting as an achiral effector. The resulting remote control is ensured by the ligand crowding tuning the stereoselectivity up to 60 % *d.e.* in the case of small size effectors.

iii) remarkably, the whole dynamic stereoselective process amplifies up to five times the chiroptical response of the free base Möbius aromatic rings highlighting a fine orchestration of the *endogenous/chiral* and *exogeneous/achiral* components of the totem.

A key point of the system is the dynamic character of the Möbius twist and bridging patterns, which rely on two different hexaphyrin conformational exchanges. The attached cyclodextrin providing a static source of chirality can either be almost silent over this process or active with the help of a remote achiral effector. This dynamic approach appears promising for the further use of Möbius chirality into all kind of stimuli responsive systems including switchable asymmetric catalysts. Work along these lines is in progress in our laboratories.

ASSOCIATED CONTENT

Supporting Information

Full experimental details and spectral data. The Supporting Information is available free of charge on the ACS Publications website.

AUTHOR INFORMATION

Corresponding Authors

* stephane.legac@univ-rennes1.fr

* mickael.menand@sorbonne-universite.fr

Author Contributions

§ These authors contributed equally.

ACKNOWLEDGMENT

We are grateful to the Agence Nationale de la Recherche for financial support (ANR research program PRALLOCAT, ANR-16-CE07-0014).

REFERENCES

- Walba, D. M.; Richards, M.; Haltiwanger, R. C. Total Synthesis of the First Molecular Möbius Strip. *J. Am. Chem. Soc.* **1982**, *104*, 3219-3221.
- For reviews, see: (a) Rzepa, H. S. Möbius Aromaticity and Delocalization. *Chem. Rev.* **2005**, *105*, 3697-3715. (b) Herges, R. Topology in Chemistry: Designing Möbius Molecules. *Chem. Rev.* **2006**, *106*, 4820-4842.
- (a) Ajami, D.; Oeckler, O.; Simon, A.; Herges, R. Synthesis of a Möbius Aromatic Hydrocarbon. *Nature* **2003**, *426*, 819-821. (b) See also: Castro, C.; Chen, Z.; Wannere, C. S.; Jiao, H.; Karney, W. L.; Mauksch, M.; Puchta, R.; van Eikema Hommes, N. J. R.; von Ragué Schleyer, P. Investigation of a Putative Möbius Aromatic Hydrocarbon. The Effect of Benzannulation on Möbius

- [4n]Annulene Aromaticity. *J. Am. Chem. Soc.* **2005**, *127*, 2425-2432.
- 4 Stępień, M.; Latos-Grażyński, L.; Sprutta, N.; Chwalisz, P.; Sztterenber, L. Expanded Porphyrin with a Split Personality: A Hückel–Möbius Aromaticity Switch. *Angew. Chem. Int. Ed.* **2007**, *46*, 7869-7873.
- 5 Sankar, J.; Mori, S.; Saito, S.; Rath, H.; Suzuki, M.; Inokuma, Y.; Shinokubo, H.; Kim, K. S.; Yoon, Z. S.; Shin, J.-Y.; Lim, J. M.; Matsuzaki, Y.; Matsushita, O.; Muranaka, A.; Kobayashi, N.; Kim, D.; Osuka, A. Unambiguous Identification of Möbius Aromaticity for meso-Aryl-Substituted [28]Hexaphyrins(1.1.1.1.1.1). *J. Am. Chem. Soc.* **2008**, *130*, 13568-13579.
- 6 Selected reviews covering the field of expanded porphyrins: (a) Sessler, J. L.; Seidel, D. Synthetic Expanded Porphyrin Chemistry. *Angew. Chem., Int. Ed.* **2003**, *42*, 5134-5175. (b) Yoon, Z. S.; Osuka, A.; Kim, D. Möbius Aromaticity and Antiaromaticity in Expanded Porphyrins. *Nat. Chem.* **2009**, *1*, 113-122. (c) Shin, J.-Y.; Kim, K. S.; Yoon, M.-C.; Lim, J. M.; Yoon, Z. S.; Osuka, A.; Kim, D. Aromaticity and Photophysical Properties of Various Topology-Controlled Expanded Porphyrins. *Chem. Soc. Rev.* **2010**, *39*, 2751-2767. (d) Stępień, M.; Sprutta, N.; Latos-Grażyński, L. Figure Eights, Möbius Bands, and More: Conformation and Aromaticity of Porphyrinoids. *Angew. Chem., Int. Ed.* **2011**, *50*, 4288-4340. (e) Saito, S.; Osuka, A. Expanded Porphyrins: Intriguing Structures, Electronic Properties, and Reactivities. *Angew. Chem., Int. Ed.* **2011**, *50*, 4342-4373. (f) Osuka, A.; Saito, S. Expanded Porphyrins and Aromaticity. *Chem. Commun.* **2011**, *47*, 4330-4339. (g) Roznyatovskiy, V. V.; Leeb, C.-H.; Sessler, J. L. π -Extended Isomeric and Expanded Porphyrins. *Chem. Soc. Rev.* **2013**, *42*, 1921-1933. (h) Tanaka, T.; Osuka, A. Chemistry of meso-Aryl-Substituted Expanded Porphyrins: Aromaticity and Molecular Twist. *Chem. Rev.* **2017**, *117*, 2584-2640. (i) Mo Sung, Y.; Oh, J.; Cha, W.-Y.; Kim, W.; Min Lim, J.; Yoon, M.-C.; Kim, D. Control and Switching of Aromaticity in Various All-Aza-Expanded Porphyrins: Spectroscopic and Theoretical Analyses. *Chem. Rev.* **2017**, *117*, 2257-2312. (j) Szyszko, B.; Białek, M. J.; Pacholska-Dudziak, E.; Latos-Grażyński, L. Flexible Porphyrinoids. *Chem. Rev.* **2017**, *117*, 2839-2909.
- 7 Heilbronner, E. Hückel Molecular Orbitals of Möbius-Type Conformations of Annulenes. *Tetrahedron Lett.* **1964**, *5*, 1923-1928.
- 8 (a) Higashino, T.; Lim, J. M.; Miura, T.; Saito, S.; Shin, J.-Y.; Kim, D.; Osuka, A. Möbius Antiaromatic Bisphosphorus Complexes of [30]Hexaphyrins. *Angew. Chem., Int. Ed.* **2010**, *49*, 4950-4954. (b) Higashino, T.; Lee, B. S.; Lim, J. M.; Kim, D.; Osuka, A. A Möbius Antiaromatic Complex as a Kinetically Controlled Product in Phosphorus Insertion to a [32]Heptaphyrin. *Angew. Chem., Int. Ed.* **2012**, *51*, 13105-13108.
- 9 (a) Oh, J.; Sung, Y. M.; Kim, W.; Mori, S.; Osuka, A.; Kim, D. Aromaticity Reversal in the Lowest Excited Triplet State of Archetypical Möbius Heteroannulenic Systems. *Angew. Chem., Int. Ed.* **2016**, *55*, 6487-6491. (b) Hong, Y.; Oh, J.; Sung, Y. M.; Tanaka, Y.; Osuka, A.; Kim, D. The Extension of Baird's Rule to Twisted Heteroannulenes: Aromaticity Reversal of Singly and Doubly Twisted Molecular Systems in the Lowest Triplet State. *Angew. Chem., Int. Ed.* **2017**, *56*, 2932-2936.
- 10 Tanaka, T.; Sugita, T.; Tokuji, S.; Saito, S.; Osuka, A. Metal Complexes of Chiral Möbius Aromatic [28]Hexaphyrin(1.1.1.1.1.1): Enantiomeric Separation, Absolute Stereochemistry, and Asymmetric Synthesis. *Angew. Chem., Int. Ed.* **2010**, *49*, 6619-6621.
- 11 Ruffin, H.; Nyame Mendendy Boussambe, G.; Roisnel, T.; Dorcet, V.; Boitrel, B.; Le Gac, S. Tren-Capped Hexaphyrin Zinc Complexes: Interplaying Molecular Recognition, Möbius Aromaticity, and Chirality. *J. Am. Chem. Soc.* **2017**, *139*, 13847-13857.
- 12 (a) Eliel, E. L.; Wilen, S. H. *Stereochemistry of Organic Compounds*; Wiley: New York, 1994. (b) Yamamoto, H.; Carreira, E. M. *Comprehensive Chirality*; Elsevier Science: Oxford, 2012.
- 13 [1.1.1.1.1.1]Hexaphyrins were discovered two decades ago independently by Cavaleiro and Osuka: (a) Neves, M. G. P. M. S.; Martins, R. M.; Tomé, A. C.; Silvestre, A. J. D.; Silva, A. M. S.; Félix, V.; Cavaleiro, J. A. S.; Drew, M. G. B. meso-Substituted Expanded Porphyrins: New and Stable Hexaphyrins. *Chem. Commun.* **1999**, 385-386 (b) Shin, J.-Y.; Furuta, H.; Yoza, K.; Igarashi, S.; Osuka, A. meso-Aryl-Substituted Expanded Porphyrins. *J. Am. Chem. Soc.* **2001**, *123*, 7190-7191.
- 14 See also: (a) Tanaka, Y.; Saito, S.; Mori, S.; Aratani, N.; Shinokubo, H.; Shibata, N.; Higuchi, Y.; Yoon, Z. S.; Kim, K. S.; Noh, S. B.; Park, J. K.; Kim, D.; Osuka, A. Metalation of Expanded Porphyrins: A Chemical Trigger Used To Produce Molecular Twisting and Möbius Aromaticity. *Angew. Chem., Int. Ed.* **2008**, *47*, 681-684. (b) Setsune, J.-i.; Tsukajima, A.; Okazaki, N.; Lintuluoto, J. M.; Lintuluoto, M. Enantioselective Induction of Helical Chirality in Cyclooctapyrroles by Metal-Complex Formation. *Angew. Chem., Int. Ed.* **2009**, *48*, 771-775. (c) Mori, T.; Tanaka, T.; Higashino, T.; Yoshida, K.; Osuka, A. Combined Experimental and Theoretical Investigations on Optical Activities of Möbius Aromatic and Möbius Antiaromatic Hexaphyrin Phosphorus Complexes. *J. Phys. Chem. A* **2016**, *120*, 4241-4248.
- 15 Wolf, C. *Dynamic Stereochemistry of Chiral Compounds: Principles and Applications*; The Royal Society of Chemistry: Cambridge, 2007.
- 16 (a) Feringa B. L. The Art of Building Small: From Molecular Switches to Motors (Nobel Lecture). *Angew. Chem. Int. Ed.* **2017**, *56*, 11060-11078. (b) Zhang L.; Marcos, V.; Leigh, D. A. Molecular Machines with Bio-Inspired Mechanisms. *Proc. Natl. Acad. Sci. USA* **2018**, *115*, 9397-9404.
- 17 (a) Clayden, J. in *Molecular Interactions – Bringing Chemistry to Life*, ed. M. G. Hicks and C. Kettner, pub. Beilstein Institut 2007, ISBN 978-3-8325-1791-5. (b) Clayden, J. Transmission of Stereochemical Information over Nanometre Distances in Chemical Reactions. *Chem. Soc. Rev.* **2009**, *38*, 817-829.
- 18 Pizzolato, S. F.; Štacko, P.; Kistemaker, J. C. M.; van Leeuwen, T.; Otten, E.; Feringa, B. L. Central-to-Helical-to-Axial-to-Central Transfer of Chirality with a Photoresponsive Catalyst. *J. Am. Chem. Soc.* **2018**, *140*, 17278-17289.
- 19 (a) Martinez, A.; Robert, V.; Gornitzka, H.; Dutasta, J.-P. Controlling Helical Chirality in Atrane Structures: Solvent-Dependent Chirality Sense in Hemicyclopentane-Oxidovanadium(V) Complexes. *Chem. Eur. J.* **2010**, *16*, 520-527. (b) Carminati, D. M.;

- Intrieri, D.; Caselli, A.; Le Gac, S.; Boitrel, B.; Toma, L.; Legnani, L.; Gallo, E. Designing ‘Totem’ C_2 -Symmetrical Iron Porphyrin Catalysts for Stereoselective Cyclopropanations. *Chem. Eur. J.* **2016**, *22*, 13599-13612.
- 20 (a) Ménand, M.; Sollogoub, M.; Boitrel, B.; Le Gac, S. Hexaphyrin-Cyclodextrin Hybrids: A Nest for Switchable Aromaticity, Asymmetric Confinement, and Isomorphic Fluxionality. *Angew. Chem., Int. Ed.* **2016**, *55*, 297-301. (b) Le Gac, S.; Boitrel, B.; Sollogoub, M.; Ménand, M. Protonated Hexaphyrin-Cyclodextrin Hybrids: Molecular Recognition Tuned by a Kinetic-to-Thermodynamic Topological Adaptation. *Chem. Commun.* **2016**, *52*, 9347-9350. (c) Ménand, M.; Sollogoub, M.; Boitrel, B.; Le Gac, S. Cyclodextrin-Sandwiched Hexaphyrin Hybrids: Side-to-Side Cavity Coupling Switched by a Temperature- and Redox-Responsive Central Device. *Chem. Eur. J.* **2018**, *24*, 5804-5812.
- 21 See reference 20b and the corresponding SI for a definition of the R_p and S_p stereodescriptors.
- 22 See reference 6d for a definition of M and P stereodescriptors. For detailed mechanistic studies of the twisting process (DFT calculations), see: (a) Marcos, E.; Anglada, J. M.; Torrent-Sucarrat, M. Theoretical Study of the Switching between Hückel and Möbius Topologies for Expanded Porphyrins. *J. Phys. Chem. C* **2012**, *116*, 24358-24366. (b) Marcos, E.; Anglada, J. M.; Torrent-Sucarrat, M. Effect of the meso-Substituent in the Hückel-to-Möbius Topological Switches. *J. Org. Chem.* **2014**, *79*, 5036-5046.
- 23 Calculated for meso-hexakis(pentafluorophenyl)[28]hexaphyrin, see: Kim, K. S.; Yoon, Z. S.; Ricks, A. B.; Shin, J.-Y.; Mori, S.; Sankar, J.; Saito, S.; Jung, Y. M.; Wasielewski, M. R.; Osuka, A.; Kim, D. Conformational Changes of meso-Aryl Substituted Expanded Porphyrins upon Protonation: Effects on Photophysical Properties and Aromaticity. *J. Phys. Chem. A* **2009**, *113*, 4498-4506.
- 24 Calculated for a triply-linked [26]HCD hybrid, see reference 20a.
- 25 (a) Pearce, A. J.; Sinaÿ, P. Diisobutylaluminum-Promoted Regioselective De-O-benzoylation of Perbenzoylated Cyclodextrins: A Powerful New Strategy for the Preparation of Selectively Modified Cyclodextrins. *Angew. Chem. Int. Ed.* **2000**, *39*, 3610-3612. (b) Lecourt, T.; Herault, A.; Pearce, A. J.; Sollogoub, M.; Sinaÿ, P. Triisobutylaluminium and Diisobutylaluminium Hydride as Molecular Scalpels: The Regioselective Stripping of Perbenzoylated Sugars and Cyclodextrins. *Chem. Eur. J.* **2004**, *10*, 2960-2971.
- 26 Hierso, J.-C. Indirect Nonbonded Nuclear Spin-Spin Coupling: A Guide for the Recognition and Understanding of “Through-Space” NMR J Constants in Small Organic, Organometallic, and Coordination Compounds. *Chem. Rev.* **2014**, *114*, 4838-4867.
- 27 Considering a transiting C_2 -symmetric rectangular conformation, the same (degenerate) Möbius isomers are obtained from twisting one or the other identical (C_2 -symmetrically related) inverted pyrroles.
- 28 These long-side patterns are also supported by the ^{19}F NMR spectra lacking the through-space ^{19}F - ^{19}F coupling constant, and by the distribution of the *para*-fluorine atoms resonating at very similar chemical shifts for $^{\text{R}}[26]1$ ($\delta = -153.12$ and -153.21 ppm, long side/long side), vs. distinct chemical shifts for $^{\text{R}}[26]2$ and $^{\text{R}}[26]3$ ($\delta\{^{\text{R}}[26]2\} = -150.50$ and -154.20 ppm; $\delta\{^{\text{R}}[26]3\} = -150.65$ and -153.90 ppm; short side/long side).
- 29 Cho, S.; Yoon, Z. S.; Kim, K. S.; Yoon, M.-C.; Cho, D.-G.; Sessler, J. L.; Kim, D. Defining Spectroscopic Features of Heteroannulenic Antiaromatic Porphyrinoids. *J. Phys. Chem. Lett.* **2010**, *1*, 895-900.
- 30 For recent examples of conformationally locked rectangular antiaromatic [28]hexaphyrins, see: (a) Yoneda, T.; Kim, T.; Soya, T.; Neya, S.; Oh, J.; Kim, D.; Osuka, A. Conformational Fixation of a Rectangular Antiaromatic [28]Hexaphyrin Using Rationally Installed Peripheral Straps. *Chem. Eur. J.* **2016**, *22*, 4413-4417. (b) Nakai, A.; Yoneda, T.; Ishida, S.-I.; Kato, K.; Osuka, A. Aromatic and Antiaromatic Cyclophane-type Hexaphyrin Dimers. *Chem. Asian J.* **2019**, *14*, 256-260.
- 31 $^{\text{R}}[26]1$, $^{\text{R}}[26]2$ and $^{\text{R}}[26]3$ exhibit only weak CD spectra, revealing that neither the planar chirality nor the cyclodextrin chirality are significantly experienced by the 26π -system (see the SI).
- 32 In the seminal paper of Osuka (reference 10), the P/M absolute configuration of the separated enantiomers of a Pd(II) complex of a Möbius [28]hexaphyrin were misassigned. In this paper, the enantiomer labelled “2A”, exhibiting negative Cotton effect, was assigned as a P twist where careful examination of its X-ray structure reveals an M twist with unambiguous left handedness of the π -system winding. See the SI.
- 33 Whereas quantitative metalation was achieved with $\text{Zn}(\text{OTf})_2/\text{L}^2$, metalation did not go to completion with $\text{Zn}(\text{OAc})_2$, even with a large excess and prolonged heating.
- 34 For instance, a pronounced *inward* orientation of the meso-aromatic substituent *cis* to the N atom of the *twisted* pyrrole has been observed with group ten metal complexes of Möbius [28]hexaphyrins, exhibiting a significant localized twist distribution due to a constraining square planar NNNC coordination sphere; see: Mori, S.; Shimizu, S.; Taniguchi, R.; Osuka, A. Group 10 Metal Complexes of meso-Aryl-Substituted [26]Hexaphyrins with a Metal-Carbon Bond. *Inorg. Chem.* **2005**, *44*, 4127-4129.
- 35 Sharp signals were observed at 243 K, see the SI.
- 36 In the (putative) case of ‘ ZnL^n ’ oriented *inward*, short distances between e.g. the Me groups of the bound L^2 and the linker ethylenic and aromatic protons (< 5 Å) would lead to significant NOE correlations. The only NOE correlations observed with the bound L^2 indicate spatial proximity between its ‘*in*’ Me group and outer β -pyrrolic protons, in good agreement with an *exo*-coordination mode (see optimized geometries in the SI).
- 37 Considering that the detection limit of the ^1H NMR experiment is ca. 2% in the present conditions, the M/P d.r. for $^{\text{M}}[28]2.\text{ZnL}$ is higher than 98:2 (hence *d.e.* > 95 %).
- 38 Only partial metalation was achieved with L^5 .

- 1
2
3
4
5
6
7
8
9
10
11
12
13
14
15
16
17
18
19
20
21
22
23
24
25
26
27
28
29
30
31
32
33
34
35
36
37
38
39
40
41
42
43
44
45
46
47
48
49
50
51
52
53
54
55
56
57
58
59
60
- ³⁹ Mikami, K.; Shimizu, M.; Zhang, H.-C.; Maryanoff, B. E. Acyclic Stereocontrol Between Remote Atom Centers via Intramolecular and Intermolecular Stereo-Communication. *Tetrahedron*, **2001**, *57*, 2917-2951.
- ⁴⁰ For a recent example of remote control of planar chirality in a dynamic system, see: Mamiya, F.; Ousaka, N.; Yashima, E. Remote Control of the Planar Chirality in Peptide-Bound Metallomacrocycles and Dynamic-to-Static Planar Chirality Control Triggered by Solvent-Induced 3_{10} -to- α -Helix Transitions. *Angew. Chem. Int. Ed.* **2015**, *54*, 14442-14446.

Table of Content graphic

